Targeted millisecond-scale activation of cells using non-invasive Sonogenetics

Marc Duque[1*], Corinne A. Lee-Kubli[1*], Yusuf Tufail[1*], Uri Magaram[1,2], Jose Mendoza Lopez[1], Eric Edsinger[1], Aditya Vasan[3], Rani Shiao[1], Connor Weiss[1], James Friend[3] and Sreekanth H. Chalasani[1,2#]

[1] Molecular Neurobiology Laboratory, The Salk Institute for Biological Studies, La Jolla, CA 92037.

[2] Neurosciences Graduate Program, University of California San Diego, La Jolla, CA 92093

[3] Medically Advanced Devices Laboratory, Department of Mechanical and Aerospace Engineering, Jacobs School of Engineering and the Department of Surgery, School of Medicine, University of California San Diego, La Jolla, CA 92093.

* These authors contributed equally to this work and are listed alphabetically.

Corresponding author

Our understanding of the nervous system has been fundamentally advanced by light- and small molecule-sensitive proteins that can be used to modify neuronal excitability. However, optogenetics requires invasive instrumentation while chemogenetics lacks temporal control. Here, we identify a candidate channel that confers sensitivity to non-invasive ultrasound on millisecond timescales. Using a functional screen, we find that human Transient Receptor Potential A1 (*hs*TRPA1) increases ultrasound-evoked intracellular calcium levels and membrane potentials. Ultrasound, but not agonist, -evoked, gating of *hs*TRPA1, requires the N-terminal tip region, intact actin cytoskeleton, and cholesterol, implicating these features in the sonogenetic mechanism. We then use calcium imaging and electrophysiology to confirm that ultrasound-evoked responses of primary

neurons are potentiated by *hs*TRPA1. We also show that unilateral expression of *hs*TRPA1 in mouse layer V motor cortical neurons leads to ultrasound-evoked contralateral limb responses to ultrasound delivered through an intact skull. Finally, ultrasound induces *c-fos* in *hs*TRPA1-expressing neurons, suggesting that our approach can be used for targeted activation of neural circuits. Together, our results demonstrate that *hs*TRPA1-based sonogenetics can effectively and non-invasively modulate neurons within the intact mammalian brain, a method that could be extended to other cell types across species.

The reductionist approach to understanding a biological system is to identify constituent components, explore their interactions and signals, and systematically alter or perturb inputs while monitoring outputs. In the nervous system, these perturbations have been facilitated by discoveries of light- and small molecule-sensitive proteins and their variants that can be expressed in specific cell populations, thereby enabling manipulation of neural activity by light (optogenetics) or small molecules (chemogenetics)[1,2], respectively. While light can be shaped, patterned and localized[3], the opacity of biological tissues makes it difficult to target deep structures in mammals without invasive surgical procedures. Small molecules can be easily delivered to various targets, regardless of depth, but these lack the temporal precision needed to perturb cellular function on the timescales of neuronal signalling[2]. Additionally, studies evaluating use of magnetic fields to drive neuronal activation (magnetogenetics) have been controversial [4,5] and may similarly lack necessary temporal precision[6]. These reports emphasize the need for a new modality that can be used to non-invasively manipulate specific cells with millisecond precision.

Ultrasound is safe, non-invasive, and can be easily focused through thin bone and tissue to volumes of a few cubic millimetres[7,8]. Moreover, continuous or repeated pulses of ultrasound at frequencies between 250 kHz – 3 MHz have been shown to stimulate neurons in rodents and non-human primates[9-13]. Ultrasound has also been used to safely manipulate deep nerve structures in human hands to relieve chronic pain[14], as well as to elicit somatosensory[15] and visual cortex sensations[16] through the intact skull. These and other studies have revealed a wide interest in adapting ultrasound for both research and therapeutic purposes[17]. Nevertheless, the mechanisms that underlie ultrasound neurostimulation remain unclear, but may include mechanical forces [18], heating[14], and cavitation[17] *in vitro,* or indirect auditory signals within the rodent brain *in vivo*[19,20]. We and others have found evidence for involvement of mechanosensitive channels in ultrasound responses of naïve rodent neurons *in vitro*[21] and *C. elegans* neurons *in vivo*[22,23]. This provides a potential path toward the development of a broadly usable sonogenetic tool that would target exogenous proteins to specific cells, thereby rendering them sensitive to ultrasound stimuli at pressures and durations that do not affect naïve cells.

We previously showed that exogenous expression of the *C. elegans* TRP-4 mechanoreceptor enables ultrasound-sensitivity in neurons that are otherwise unresponsive to ultrasound stimulation[23]. Similar ultrasound-sensitivity has also been observed *in vitro* in cells induced to express proteins belonging to the mechanosensitive (MSC)[24], Piezo[25], Prestin[26], transient receptor potential (TRP)[21], and TREK[27] families. We therefore hypothesized that proteins from these ion channel families and others hypothesized to have mechanosensitivity might confer ultrasound sensitivity to mammalian cells. To identify an optimal candidate, we used a functional readout-based assay to screen a library of 191 candidate channels and their homologs (Table S1). We then used a combination of imaging, pharmacology, electrophysiology,

and comparative sequence analysis, as well as behavioural, and histological analyses to demonstrate that a mammalian protein, *Homo sapiens* transient receptor potential A1 (*hs*TRPA1), confers ultrasound sensitivity to cells *in vitro* and *in vivo*, thereby establishing the sonogenetic tool in mammals.

Results

*hs*TRPA1 is a sonogenetic candidate

We screened for ultrasound-triggered cellular responses by aligning an optical imaging setup with a custom designed single-crystal 6.91 MHz lithium niobate transducer (Fig. 1a) that lacks hysteresis and thereby generates minimal heat as it converts electrical input into mechanical energy[28]. We also profiled the pressure output and corresponding temperature changes in our imaging set up using a combined fibre optic probe (Supplementary Fig. 1a,b) and selected ultrasound parameters for the screen at a pressure and duration that caused minimal temperature change (100 ms, 1.5 MPa). We transiently transfected each of 191 candidate proteins (Supplementary Table 1) along with a dTomato (dTom) fluorescent reporter into human embryonic kidney-293T (HEK) cells expressing a genetically encoded calcium indicator (GCaMP6f[29]) and monitored changes in intracellular calcium upon ultrasound stimulation (Supplementary Figure 1d, e, g, h). We found that cells expressing mammalian TRPA1 channels were the most likely to respond to ultrasound, with the human homolog as the most effective candidate (Fig. 1b, Video S1). In contrast, the mouse homolog was only a third as responsive as *hs*TRPA1, and non-mammalian variants were insensitive to ultrasound (Fig. 1c). None of the other proteins tested in our screen showed significant sensitivity to ultrasound parameters used in our screen, including channels previously shown to respond to ultrasound stimuli at different

frequencies, pressures, or duration (Fig. 1c). While we confirmed functional overexpression of Piezo1 and TRPV candidate channels (Supplementary Fig. 1k,l), we cannot rule out the possibility that other tested proteins did not perform due to issues with expression, trafficking, or folding.

We next confirmed that ultrasound responsiveness was due to direct activation of *hs*TRPA1. We first visualized *hs*TRPA1 using immunohistochemistry and found that it was indeed expressed only in dTom+ cells and trafficked to the HEK plasma membranes (Fig. 1d), where it co-localized with membrane-targeted EGFP-CAAX[30]. Consistently, we found that HEK cells expressing *hs*TRPA1 were selectively activated by ultrasound stimulation in a pressure- and duration-dependent manner (Supplementary Fig. 1c-e), while dTom-only control cells showed no response to ultrasound stimulation (Supplementary Fig. 1g, h, Video S2). Moreover, we found that the TRPA1-selective agonists N-methylmaleimide (NMM) and allyl isothiocyanate (AITC)[31] also specifically activated TRPA1-expressing HEK cells, confirming that the channel was indeed functional (Fig. 1f, Supplementary Fig. 1f, i, j). Finally, the TRPA1 antagonist HC-030331[32] inhibited ultrasound responses in *hs*TRPA1-expressing cells (Fig. 1f). Collectively, these results show that the ultrasound responses require gating of *hs*TRPA1, which facilitated increased intracellular calcium.

Next, we used electrophysiological methods to monitor changes in the membrane conductance of excitable HEK cells[33] expressing *hs*TRPA1 or dTom-only control. To increase our recording efficiency, we used a cell-attached configuration (Fig. 1g), wherein we were able to maintain suitable access and membrane resistance while exposing cells to ultrasound stimuli. We found that cells expressing *hs*TRPA1 had higher basal rates of activity (Supplementary Fig. 2a) but no significant disruptions in their I-V curve compared to controls (Supplementary Fig.

2b), confirming that channel expression did not alter membrane properties. Furthermore, negative currents in response to ultrasound were significantly larger and more numerous in *hs*TRPA1-expressing cells compared to controls (Fig. 1h; Supplementary Fig. 2c, d). These ultrasound-triggered currents were of similar magnitude as those previously observed for pharmacological activation of the TRPA1 channel[34]. Furthermore, we found that ultrasound-triggered membrane events were attenuated by the TRPA1 antagonist, HC-030301, confirming a specific role for *hs*TRPA1 (Fig. 1i). Taken together, these results show that short ultrasound pulses can selectively lead to opening of *hs*TRPA1 channels, resulting in a rapid increase of intracellular calcium in HEK cells.

Putative mechanisms underlying ultrasound sensitivity of TRPA1

Multiple studies have shown that TRPA1 is a widely conserved calcium permeable non-selective cation channel that is involved in detecting a wide-range of exogenous stimuli including electrophilic compounds that interact with the nucleophilic amino acids in the channel, small peptides that partition in the plasma membrane, cold, heat, and others, although sensitivity to different stimuli varies across species (reviewed by[35]). Despite this broad sensitivity and a resolved cryo-electron microscopy structure, the underlying mechanisms of TRPA1 activation are only recently being elucidated. For example, a scorpion toxin peptide (WaTx) has been shown to activate TRPA1 by penetrating the lipid bilayer to access the same amino acids bound by electrophiles, thereby stabilizing the channel in an active state and prolonging channel opening[36]. In contrast, electrophilic irritants have been shown to activate the TRPA1 channel using a two-step cysteine modification that widens the selectivity filter to enhance calcium permeability and open the cytoplasmic gate[37]. These studies suggest that the TRPA1 channel

might interact with the cytoskeleton and components of the membrane bilayers, including cholesterol, to transduce signals.

Structurally, TRPA1 comprises an intracellular N-terminal tip domain, 16 ankyrin repeats, 6 transmembrane domains and an intracellular C-terminal domain (Supplemental Figure 3a). To identify TRPA1 domains critical for ultrasound sensitivity, we compared sequences of each domain in the human protein to its ultrasound-sensitive mammalian and ultrasound-insensitive non-mammalian chordate TRPA1 homologs (Supplementary Fig. 3b, Table S2). We expected that *hs*TRPA1 domains and motifs that are particularly conserved among mammals specifically may be crucial for ultrasound sensitivity. Sequence analysis of *hs*TRPA1 and the 9 additional homologs we tested revealed that the N-terminal tip region is highly conserved in the mammalian compared to non-mammalian chordate species that we tested (58% vs 13% identity, respectively, Fig. 2a), particularly the first 22 amino acids (87% vs 17% identity, respectively, Supplementary Fig. 3c). Therefore, we hypothesized that the N-terminal tip region might be important for mediating ultrasound sensitivity. Indeed, deletion of this region (Δ1-61) from *hs*TRPA1 completely abolished responses to ultrasound (Fig. 2b), while having no effect on responses to chemical agonist (Fig. 2c).

Next, we focused on the N-terminal ankyrin repeats that have been hypothesized to interact with cytoskeletal elements and act as a gating spring in response to mechanical force[38,39]. We found that deleting all 16 ankyrin repeats, while leaving the N-terminal tip region intact, completely abolished responses to both ultrasound and chemical agonist (Fig. 2c, d); however, we could not confirm whether this channel was expressed and properly trafficked to the membrane. We then used sequence homology to guide a more targeted ankyrin deletion. Ankyrin repeat 12 is highly conserved within mammalian species (97% identity), and is the most highly

conserved ankyrin repeat in the non-mammalian species we tested (74% identity, Table S2, Supplementary Fig. 3d). Consistently, ΔANK12 did not respond to either ultrasound or AITC (Fig. 2b, c), suggesting that it is required for normal channel function. In contrast, Ankyrin repeat 1 is the least conserved mammalian ankyrin repeat domain (46% identity; Table S2, Supplementary Fig. 3e), and we observed no impairment in ΔANK1 *hs*TRPA1 responsiveness to either ultrasound or AITC (Fig. 2b,c). Taken together, our results suggest that the cytoplasmic ankyrin portion of the channel is important for ultrasound sensitivity conferred by *hs*TRPA1, likely through an interaction governed by the N-terminal tip region.

Ankyrin repeat regions from *Drosophila* NOMPC (TRPN) are thought to be important in mechanosensation due to their interactions with microtubules [40]. Therefore, we probed the involvement of cytoskeletal elements in ultrasound sensitivity of *hs*TRPA1. We found that treating *hs*TRPA1-expressing HEK cells with the actin depolymerizing agents, cytochalasin D and latrunculin A, reduced their ultrasound responses compared to vehicle or an actin stabilizing agent, jasplakinolide (Fig. 2d). In contrast, disrupting or stabilizing microtubules with nocodazole or Taxol, respectively, had no significant effect on ultrasound-evoked *hs*TRPA1 responses (Fig. 2d). Immunohistochemistry confirmed that destabilizing treatments did indeed disrupt the actin cytoskeleton and microtubules (Supplementary Fig. 4a, b). Moreover, we found that AITC- triggered responses were not altered by treatment with either cytochalasin D or nocodazole, although they were significantly reduced by latrunculin A, jasplakinolide, and paclitaxel (Supplementary Fig. 4c). Therefore, actin depolymerisation by cytochalasin D treatment selectively blocked *hs*TRPA1 responses to ultrasound, but not chemical agonist, demonstrating a specific role for the actin cytoskeleton in ultrasound sensation.

Mouse TRPA1 has been hypothesized to localize to lipid rafts through a mechanism governed by a cholesterol recognition/interaction amino acid consensus sequence (CRAC) domain within the transmembrane helix 2 of TRPA1[41]. Interestingly, we identified a CRAC motif (L/V-(X)(1-5)-Y-(X)(1-5)-R/K, where X are non-polar residues) in transmembrane helix 2 that was highly similar in all tested mammals, but that was absent in reptiles and heavily modified in fish (Fig 2e). Therefore, we hypothesized that interactions with cholesterol might be important for ultrasound responsiveness of *hs*TRPA1 channels. We therefore depleted cellular membrane cholesterol with methyl-beta-cyclodextrin (MCD)[42], and found that this attenuated *hs*TRPA1 responses to ultrasound, but did not affect the response to AITC (Fig. 2f).

Given that the interaction between *hs*TRPA1 and cholesterol is likely important for ultrasound sensitivity, we speculated that the state of the membrane surrounding *hs*TRPA1 might modulate its activity. Interestingly, mammalian TRPA1 channels do not seem to be activated by membrane tension as observed for standard mechanosensitive channels[43,44]. In contrast, the amphipathic tarantula toxin peptide, GsMTx-4, which inhibits most mechanosensitive channels[45,46], activates mammalian TRPA1[47,48]. We further tested GsMTx-4-mediated activation of TRPA1 homologs and discovered a correlation between GsMTx-4 sensitivity and ultrasound responsiveness in HEK cells. Mammalian TRPA1 channels were activated by both GsMTx-4 and ultrasound, fish TRPA1 showed limited sensitivity to both, while reptile TRPA1, Piezo and TRPV1 did not respond (Supplementary Fig. 5a, Supplementary Fig. 1j.k). In contrast, all TRPA1 homologs responded to the TRPA1 agonist AITC (Supplementary Fig. 5b), indicating that each channel is functional in HEK cells. Furthermore, GsMTx-4 also had no effect on *hs*TRPA1-expressing cells that had been treated with MCD (Supplementary Fig. 5c), indicating that the putative interaction with cholesterol is important for sensing both ultrasound and

GsMTx-4. Taken together, these results suggest that *hs*TRPA1 may use a distinct mechanism from classically mechanosensitive proteins to sense ultrasound-triggered membrane perturbations, potentially through interactions with cholesterol-rich domains in the bilayer. While the precise molecular mechanism of TRPA1 responsiveness to ultrasound remains elusive, our studies suggest a role for ankyrin repeats, the actin cytoskeleton, and cholesterol in driving ultrasound-evoked *hs*TRPA1 responses.

*hs*TRPA1 potentiates ultrasound-responses in primary neurons

To test whether *hs*TRPA1 can also render neurons sensitive to ultrasound stimuli, we infected embryonic day 18 (E18) mouse primary cortical neurons with adeno-associated viral (AAV) vectors expressing either Cre-dependent *hs*TRPA1 or Cre-only control along with a genetically encoded calcium indicator, GCaMP6f[29] (Fig. 3a). Consistent with previous studies[49], we did not detect *hs*TRPA1 RNA in dorsal root ganglia (DRG) or brain from E18 mice (Supplementary Fig. 6e, f). We confirmed functional expression of *hs*TRPA1 in infected neurons by monitoring their responses to AITC, and likewise observed that Cre-only control neurons did not respond to AITC (Supplementary Fig. 7a). Consistent with our HEK cell results, we found that ultrasound triggered a significant increase in intracellular calcium in *hs*TRPA1-expressing neurons (Fig. 3b, Video S3). Cre-expressing neurons showed some calcium responses to ultrasound, but these were significantly lower in magnitude than those observed in *hs*TRPA1-expressing neurons (Supplementary Fig. 7b, c, Video S4). Both *hs*TRPA1 and control Cre-expressing neurons showed increased responses to longer (Fig. 3c) and more intense ultrasound stimuli (Fig. 3d), though *hs*TRPA1-expressing neurons showed greater sensitivity, confirming that *hs*TRPA1 expression enhances neuronal responses to ultrasound. Response latency was

significantly reduced, while the duration of responses was increased as ultrasound pressures increased (Supplementary Fig 8a, b). The majority of *hs*TRPA1-expressing had a response latency within 500-900ms of stimulus onset, while response durations ranged from 2-30 s (Supplementary Fig. 8c, d). Moreover, *hs*TRPA1-expressing neurons could be stimulated repeatedly without apparent deleterious effects on cell health or a substantial decrement in calcium flux (Fig. 3e Video S5), with cells returning to baseline after stimulation.

Next, we probed whether ultrasound-mediated effects in control and *hs*TRPA1-expressing neurons were due to TRPA1. Treating *hs*TRPA1 expressing neurons with HC-030331, significantly attenuated their responses to ultrasound, but had no effect on the ultrasound-evoked activity in control neurons (Fig. 2f). Furthermore, cortical neurons cultured from TRPA1-/- mice also responded to ultrasound (Supplementary Fig. 7d), indicating that even undetectable levels of TRPA1 in neurons or astrocytes likely do not account for ultrasound responses in control neurons. Moreover, the sodium channel blocker, tetrodotoxin, partially blocked ultrasound responses in *hs*TRPA1 neurons, while completely abolishing responses in control neurons (Fig. 3f). We also found that sequestering extracellular calcium with BAPTA blocked neuronal responses to ultrasound (Supplementary Fig. 8e). In contrast, treating neurons with a TRPV1 antagonist had no effect on their ultrasound responses (Supplementary Fig. 8e), thereby ruling out the contribution of this heat-responsive channel to ultrasound sensitivity in TRPA1-expressing neurons either directly or through a synergistic interaction[50]. These results show that ultrasound can directly activate AAV9-*hs*TRPA1 transduced neurons, leading to intracellular calcium influx, which may be amplified by voltage-gated sodium channels. In contrast, ultrasound responses in control neurons are due to a TRPA1-independent mechanism.

We then used electrophysiological methods to confirm the role of *hs*TRPA1 in mediating ultrasound-evoked neuronal responses. We encountered difficulties with unstable current responses due to variable membrane resistances and diminished recording times in the cell-attached configuration we used with the excitable HEK cells (Fig.1g). To overcome this, we used the whole-cell patch clamp configuration (Fig. 3g), which allowed us to obtain stable membrane resistances and reliable measurements when access and membrane resistance were maintained during ultrasound stimulation trials. Similar to our HEK cell experiments, we found that AAV-mediated *hs*TRPA1 expression did not alter neuronal membrane properties (Supplementary Fig. 9a). Cre-expressing control neurons retained intrinsic responsiveness to ultrasound, consistent with previous studies[10,21]. However, *hs*TRPA1-expressing neurons showed larger current responses (>500 pA) compared to controls within a few milliseconds of ultrasound stimulation (Fig. 3h, i). Together, we find that *hs*TRPA1 confers enhanced responses to ultrasound compared to controls as assessed by their relative responses, magnitude of peak responses and area under the curve metrics (Fig. 3j-l).

*hs*TRPA1 confers ultrasound sensitivity *in vivo*

We next determined whether *hs*TRPA1 can be used as a sonogenetic tool for temporally-selective activation of neurons *in vivo*. To this end, we used Cre-dependent AAV to restrict the expression of hsTRPA1 to layer V motor cortical neurons in Npr-3 Cre transgenic mice[51] (Fig. 4a). We first used *in situ* hybridization to confirm that adult cortical neurons do not express endogenous TRPA1 (Supplementary Fig. 6). Using coordinates based on a previous study[52], we co-injected AAV encoding myc-tagged *hs*TRPA1 with AAV encoding GFP to visualize the transfected neurons into the left motor cortex. This approach robustly transduced layer V cortical

neurons throughout the forelimb and hindlimb motor cortices (Fig. 4b, Supplementary Fig. 10a) and their projections in the right cervical and lumbar spinal cord (Supplementary Fig. 10b)[53]. Using the 6.91 MHz lithium niobate transducer coupled to the exposed skull through ultrasound gel, we verified our ability to deliver ultrasound to cortical regions. This *in vivo* approach delivered peak negative pressures ranging from 0.35-1.05 MPa with minimal temperature changes (Supplementary Fig. 11).

After 2-4 weeks following intracranial injection, we monitored ultrasound-evoked electromyography (EMG) responses in the bilateral biceps brachii and biceps femorii muscles. Ultrasound evoked few EMG responses and no visible movements in any of the limbs of GFP-control mice (Fig. 4d-f). In contrast, animals injected with AAV9-*hs*TRPA1 in the left motor cortex showed dose-dependent EMG responses and visible movement in their right fore- and/or hindlimbs (Fig. 4d, e, Video S6). EMG responses in the left forelimb occurred infrequently, suggesting circuit specific sensitivity to ultrasound (Fig. 4f). Consistently, we also observed some of the transduced cortical neuron processes innervating the left forelimb motor pools (Supplementary Fig. 10d). Moreover, while most EMG responses occurred within 1 second of ultrasound stimulation, the latency and duration of these responses increased with stimulus duration (Fig. 4g, h). To confirm functional activation of cortical neurons, we then tested whether ultrasound stimulation increased c-fos in motor cortical neurons expressing *hs*TRPA1. While ultrasound stimulation had no effect on the number of c-fos positive cells in animals expressing GFP, it significantly increased the number of c-fos positive cells in cortical motor neurons of *hs*TRPA1-expressing mice (Fig. 4i-k, Supplementary Fig. 12b). This upregulation was specific to the cortex and we did not detect increased c-fos in the auditory cortex in these

animals (Supplementary Fig. 12c-f), suggesting that the ultrasound-mediated effect does not involve incidental activation of the auditory cortex as has been previously suggested [19,20].

We could reliably activate both *in vitro* and *in vivo* neural circuits using sonogenetics. To assess its safety *in vivo*, we studied two metrics of safety, the effect of cortical TRPA1 expression on a motor learning task and the effect of sustained ultrasound delivery on integrity of the blood-brain barrier. We found that both *hs*TRPA1- and GFP-expressing animals had comparable ability to learn the rotarod task (Supplementary Fig. S12a). Similarly, we found that animals receiving 1 hour of intermittent ultrasound stimulation had no damage to their blood brain barrier. In contrast to stab wound positive control animals in which both 10kDa fluorescent dextran accumulated and mouse IgG showed elevated binding, no increase in fluorescence was observed in animals receiving ultrasound, indicating that neither large nor small proteins were able to leak through the blood brain barrier during sonication (Supplementary Fig.13). Taken together, these results show that ultrasound can be used to selectively modulate neurons infected with AAV9-*hs*TRPA1 through an intact mouse skull at a frequency and pressure that neither affects normal behaviour nor causes blood-brain barrier impairment.

Discussion

We demonstrate that *hs*TRPA1 is a candidate sonogenetic protein that confers ultrasound sensitivity to mammalian HEK cells and rodent neurons *in vitro* and *in vivo*. Using an unbiased screen, we found that *hs*TRPA1-expressing HEK cells show ultrasound-evoked calcium influx and membrane currents. Moreover, we reveal critical components of *hs*TRPA1 ultrasound sensitivity, including the N-terminal tip region and interactions with the actin cytoskeleton and cholesterol. We also show that *hs*TRPA1 potentiated ultrasound-evoked calcium transients in

rodent primary neurons. In addition, we used *hs*TRPA1 to selectively activate neurons within an intact mouse skull, using single pulses of ultrasound ranging from 1-100 ms. These ultrasound parameters are below the range associated with cavitation effects[54]. Accordingly, we observed no damage to the blood brain barrier even with intermittent ultrasound delivered over 60 minutes. Moreover, overexpressing *hs*TRPA1 did not cause behavioural changes on rotarod assays, confirming the viability of this candidate protein for sonogenetics use in rodent experiments.

Ultrasound has been shown to have neuromodulatory effects in mice[10,11], non-human primates[12,13], and even human subjects[15,16], while the underlying mechanisms remain poorly understood. We previously showed that overexpressing the mechanosensory receptor TRP-4 (a TRP-N homolog) in *C. elegans* neurons renders them sensitive to short pulses of ultrasound, identifying the first putative sonogenetic candidate[23]. Multiple groups have since identified additional ultrasound-sensitive candidates including MscL[24], Prestin[26], Piezo[25], TREK[27], MEC-4[22], TRPC1, TRPP2, and TRPM4[21] using *in vitro* assays, but demonstration of their activity *in vivo* has been elusive. We identified *hs*TRPA1 and its mammalian homologs as top hits in an unbiased screen from a curated library of candidate proteins, emphasizing the unique nature of this protein.

Previous studies have shown that ankyrin repeats form a super helical coil that could act as springs for mechanosensitive gating in NOMPC/TRPN1[39]. We show that the TRPA1 N-terminal tip domain might be critical for ultrasound sensitivity, and is highly similar in mammalian TRPA1 variants that showed sensitivity to ultrasound, but varies across non-mammalian chordate TRPA1 homologs that did not. We further show that an intact actin cytoskeleton is required for *hs*TRPA1 ultrasound responses. Consistently, previous studies have shown that the actin cytoskeleton can either directly interact with mechanosensitive channels[55] or

interact with the plasma membrane to modify mechanosensation[56]. We therefore speculate that the *hs*TRPA1 N-terminal tip region may interact with the actin cytoskeleton to transduce ultrasound-induced membrane perturbations into changes in intracellular calcium. Our analysis of TRPA1 sequences across homologs further suggests that a CRAC domain that is thought to mediate interactions with cholesterol[41] is heavily modified or missing from the second transmembrane domain of ultrasound-insensitive variants. Indeed, we found that interaction with the lipid bilayer is critical for ultrasound sensitivity of *hs*TRPA1 as treating *hs*TRPA1-expressing cells with MCD, which removes cholesterol, attenuated their responses to ultrasound but not to a chemical agonist.

In turn, the ultrasound sensitivity of mammalian TRPA1 may be linked to its sensitivity to compounds that distort the lipid membrane, including GsMTx-4, trinitrophenol, and bacterial lipopolysaccharide[47,57]. Indeed, responsiveness to GsMTx-4 across reptilian, fish, and mammalian variants was correlated to ultrasound sensitivity, suggesting a potential common mechanism. This is consistent with previous data showing that polyunsaturated fatty acids that alter membrane fluidity activate mammalian, but not non-mammalian, homologs of TRPA1, similar to ultrasound[48]. Crucially, *hs*TRPA1 sensitivity to GsMTx-4 is disrupted by incubation with MCD, suggesting that responsiveness to both GsMTx-4 and ultrasound depend upon TRPA1 interactions with cholesterol. Recent studies have also shown that ultrasound can not only deflect membranes or induce cavitation, but also have complex effects on the lipid bilayer via acoustic radiation forces, turbulence, and shear stress[18,58]. We suggest that *hs*TRPA1 might respond to ultrasound-triggered perturbation of the lipid bilayer along with other mechanical effects on the cell.

Previous studies have shown that naïve neurons can respond to ultrasound, both *in vitro*[21] and *in vivo*[10]. Similarly, we observe that the ultrasound parameters we use can also activate naïve neurons *in vitro*. However, these responses are significantly smaller than those observed in *hs*TRPA1-expressing neurons. Moreover, we find that ultrasound responses in control neurons are unlikely to be TRPA1-mediated, as these are not reduced upon treatment with TRPA1 antagonists, and because neurons cultured from TRPA1-/- mice also responded to ultrasound. Accordingly, we did not detect endogenous TRPA1 in E18 brain tissue. Together, these results suggest that intrinsic neuronal responses to our ultrasound parameters are unlikely to involve TRPA1 in neurons or, as has been suggested at lower ultrasound frequencies, in astrocytes[59]. Instead, a recent study found that knocking down TRPP1, TRPP2, Piezo, TRPC1, and TRPM4 each partially reduce ultrasound-evoked neuronal responses[21]. We also show that blocking voltage-gated sodium channels eliminated neuronal ultrasound induced responses. Therefore, intrinsic ultrasound neuromodulation may involve a number of ion channels whose activity is further amplified by voltage-gated sodium channels. We show that *hs*TRPA1-expressing neurons maintain partial ultrasound sensitivity in the presence of a sodium-channel blocker, confirming that *hs*TRPA1-mediated ultrasound sensitivity is at least partially independent from the mechanism contributing to ultrasound activation in control neurons.

Finally, we demonstrate that *hs*TRPA1 can be used to selectively activate a specific cell population *in vivo* with ultrasound pulses (1-100 ms) from a 6.91 MHz transducer. We have not tested additional ultrasound frequencies, which may explain why our screen did not identify previously published candidates[24-26]. Our data hint that ultrasound might not act as a simple stretch force on the membrane, and that channels that likewise sense other perturbations, including lipid bilayer changes, could be good candidates for sonogenetics. Moreover, our

identification of specific interactions (namely, actin, lipid bilayers) and the N-terminal tip domain in *hs*TRPA1 will allow us to rapidly engineer this channel for enhanced ultrasound sensitivity and ion permeability. Broadly speaking, we suggest that *hs*TRPA1 and its variants could be used to non-invasively control neurons and other cell types across species.

Methods

Animal husbandry. Studies were performed using a total of 50 adult mice including both males and females. Animals were group housed in an American Association for the Accreditation of Laboratory Animal Care approved vivarium on a 12 hour light/dark cycle, and all protocols were approved by the Institutional Animal Care and Use Committee of the Salk Institute for Biological Studies. Food and water were provided ad libitum, and nesting material was provided as enrichment. Colonies of C57Bl6/J (JAX# 000664), Npr3-cre[51] (JAX# 031333), TRPA1 knockout[60] (JAX #006401) mice were maintained for experiments.

HEK cell culture and transfection. HEK cells expressing human αvß3 integrin[61] were cultured in DMEM supplemented with 10% FBS and 20mM glutamine in a 5% CO2 incubator. A stable calcium reporter line was generated with a GCaMP6f lentivirus (Cellomics Technology PLV-10181-50) followed by FACS sorting. For screening experiments and characterization of each candidate channel, GCaMP6f-expressing HEK cells were seeded on 12-well cell culture plates with 18mm glass coverslips coated with PDL (10µg/µl; Sigma-Aldrich P6407) for 1-2h. Coverslips were washed with Milli-Q water and cells seeded at a density of 250000 cells/well. Cells were transfected with Lipofectamine LTX Reagent (ThermoFisher 15338100) according to the manufacturer's protocol and 24h after plating, using 500ng DNA of the clone of interest for

each well. Cells were kept at 37°C for an additional 24 hours before imaging on our ultrasound stimulation setup.

Ultrasound transducer: We used a set of custom-made single crystalline 127.68 Y-rotated X-propagating lithium niobate transducers operating in the thickness mode, as described in[28]. The fundamental frequency was measured to be 6.91 MHz using non-contact laser Doppler vibrometry (Polytec, Waldbronn, Germany). The devices were diced to 12 mm x 12 mm and built in to the *in vitro test* setup. The transducers were coated with a conductive layer of Au with a thickness of 1 μm with 20 nm of Ti acting as an adhesion layer. A DC sputtering (Denton 635 DC Sputtering system) process was used to coat 4" wafers in an inert gas environment with a 2.3 mTorr pressure and rotation speed of 13 rpm, at a deposition rate of 1.5 A/s for Ti and 7A/s for Au. Devices were diced to size using an automated dicing saw (DISCO 3220) and the resonance frequency verified using non-contact laser Doppler vibrometry.

Imaging rig for ultrasound stimulation. We upgraded an existing upright epi-fluorescent Zeiss microscope to perform a monolayer two-dimensional screen. For this application we used our custom-made 12x12mm lithium niobate transducer placed in a heated stage fixture underneath the cell chamber. Stimulus frequency and duration were controlled by a waveform generator (Keysight 33600A Series), and pressure was controlled through a 300-W amplifier (VTC2057574, Vox Technologies, Richardson, TX). Simultaneous calcium imaging was performed using a 40x water dipping objective at 16.6 frames per second with an Orca Flash 4.0 camera and a GFP filter.

Candidate channel screen. We generated a library of candidate channels that was initially based on a literature survey of naturally occurring ion channels and other membrane proteins that have been suggested to display mechanosensitive or ultrasound sensitive properties[23-26,62,63]. From this initial list, related channels and variants from different species were selected, resulting in a final set of 191 proteins (Supplementary Table S1). Each channel was cloned into a custom bicistronic pcDNA3.1(+) vector using a porcine teschovirua-1 2A self-cleaving peptide (p2A) sequence, expressing the channel and the fluorescent protein dTomato under a human cytomegalovirus (CMV) promoter. All plasmids were generated by Genscript Biotech (New Jersey, United States).

***In vitro* pharmacology**. For inhibition of TRPA1, we incubated cells with the antagonist HC030031[59] (40μM in DMSO; Cayman Chemicals #11923) for 45 min before stimulation. For activation of TRPA1, we used NMM[59] (N-Methylmaleimide; 100μM in DMSO Sigma-Aldrich #389412) or AITC[31] (30μM in DMSO, allyl isothiocyanate; Sigma-Aldrich # 377430). For activation of Piezo1, we used yoda-1[64] (10μM in DMSO; Tocris #5586). For activation of TRPV1 we used capsaicin[65] (3μM in DMSO; Sigma-Aldrich #M2028). The final concentration of DMSO in the external solution was 0.1% or lower for all groups; which was also used as vehicle control. GsMTx-4[47] (1μM in water; Alomone Labs # STG-100) was used to stimulate TRPA1. For cytoskeleton experiments, nocodazole (5μM; Tocris, #1228), jasplakinolide (200μM; ThermoFisher # J7473), paclitaxel (600nM; Sigma-Aldrich # T7191), cytochalasin D (5μM; Cayman Chemicals, #11330) or latrunculin A (1μM; Cayman Chemicals, # 10630) in 0.1% DMSO were added to the culture media 45 minutes prior to imaging[40]. For pharmacology in primary neurons, we used TRPV1 antagonist, A784168[66] (20μM; Tocris, #4319, 45 min

incubation) in 0.1% DMSO, BAPTA[67] (30μM; Invitrogen, #B1204, 45 min incubation) directly dissolved in culture media and TTX[68] (18μM; tetrodotoxin citrate; Tocris #1069, 5 minute incubation, where we also inhibit TTX-R channels).

Sequences and annotations: Ten TRPA1 peptide sequences were retrieved from the National Center for Biotechnology Information (NCBI) RefSeq database for human (*Homo sapiens*; NCBI Taxonomy 9606; RefSeq XP_016869435.1), mouse (*Mus musculus*; NCBI Taxonomy 10090; RefSeq NM_177781), beaver (*Castor canadensis* ; NCBI Taxonomy 51338; RefSeq XP_020010675.1), alpaca (*Vicugna pacos*; NCBI Taxonomy 30538; RefSeq XP_006202494.1), donkey (*Equus asinus*; NCBI Taxonomy 9793; RefSeq XP_014709261.1), bat (*Eptesicus fuscus*; NCBI Taxonomy 29078; RefSeq XP_008148609.1), alligator (*Alligator mississippiensis*; NCBI Taxonomy 8496; RefSeq XP_006277080.1), snake (*Notechis scutatus*; NCBI Taxonomy 8663; RefSeq XP_026545023.1), molly (*Poecilia formosa*; NCBI Taxonomy 48698; RefSeq XP_007554661.1), and zebrafish (*Danio rerio*; NCBI Taxonomy 7955; RefSeq NP_001007066.1). The human TRPA1 sequence was also retrieved from the UniProtKB database and aligned to the human TRPA1 RefSeq sequence to confirm that the sequences were identical. Uniprot coordinates of major domains and features for human TRPA1 were used to annotate the sequence in Geneious Prime (version 2020.1.2).

Phylogenetic analysis. A multiple sequence alignment of all ten TRPA1 sequences was generated using Geneious Prime MAFFT (version 7.450)[69], with a BLOSOM 62 scoring matrix, gap open penalty of 1.53, and offset value of 0.123. A phylogenetic gene tree based on the MAFFT alignment was generating using Geneious Prime RAxML (version 8.2.11)[70], with a

GAMMA BLOSOM 62 protein model, bootstrapping using rapid hill-climbing with seed 1, starting with a complete random tree, and using the maximum likelihood search convergence criterion. The maximum likelihood tree was assessed and annotated in FigTree (version 1.4.4).

Consensus sequence and percent identity. Consensus sequences for the 10 tested chordate, mammalian, and non-mammalian alignments, each having *hs*TRPA1 as reference, were generated in Geneious Prime. Threshold for consensus was set to 65%, as this ensured contribution from both mammalian and non-mammalian sequences for chordate, from rodents, ungulates, and bats for mammalian, and from reptiles and fishes for non-mammalian alignments. Alignment and consensus sequences were annotated in Geneious Prime to highlight either agreement or disagreement of a given amino acid relative to human TRPA1. Percent identity of consensus sequence to human was calculated to quantify the degree of sequence conservation or divergence in the chordate, mammalian, non-mammalian species.

CRAC-CARC motif annotation. CRAC ([LV]X(1,5)YX(1,5)[RK]) and CARC ([RK]X(1,5)[YF]X(1,5)[LV]) motifs, as defined in[71] were annotated per TRPA1 sequence using the Geneious Prime EMBOSS 6.5.7 fuzzpro tool[72].

Constructs of ankyrin TRPA1 mutants. To generate ankyrin repeat deletion constructs, a PCR based approach was used. Bicistronic constructs co-expressing deletion mutants and dTom were synthesized by Genscript Biotech (New Jersey, United States). For ΔANK1-16, amino acids (aa) 97-608(Ref seq. UniProtKB - O75762) were deleted, corresponding to nucleotide deletions 2731-4266 (Ref seq. XM_017013946.1). For the rest of constructs the aa and nucleotide

deletions were as follows: ΔN-tip: aa deletions 1-61, ΔANK12: aa deletions 445-479, nucleotide deletions 3775-3879; ΔANK1: aa deletions 67-95, nucleotide deletions 2641-2727.

***In vitro* electrophysiology.** A stable line of HEK cells expressing Nav1.3 and Kir2.1 (Ex-HEK[33], ATCC CRL-3269) were cultured on 18mm round coverslips, at a seeding density of ~300k cells/well in a tissue-culture treated 12-well plate. Cells were transiently transfected with a custom plasmid (Genscript) expressing hsTRPA1 and dTom fluorescent reporter as for screening experiments, 18-24 h post seeding. Cells underwent a media change, were allowed to recover, and then were used for recordings 18-24 h after transfection. Coverslips were transferred to a custom machined acrylic stage containing a bath of external solution; NaCl (140 mM), KCl (4 mM), $MgCl_2$ (2 mM), Glucose (5 mM) and HEPES (10 mM) with an osmolarity of ~290 mOsm. Patch pipettes were pulled on a Sutter puller model P-97 programmed to give 4-6 MΩ tips from filamented borosilicate glass (o.d. 1.5 mm, i.d. 0.86 mm). Internal solution was CsF or KF based and obtained from Nan]i[on (#08 3008, #08 3007). An Olympus 40x water dipping lens with 0.8 NA was used in combination with a (QImaging OptiMOS) cMOS camera used to visualize cells with Köhler or fluorescent illumination. dTom signal was used to confirm *hs*TRPA1 expression in HEK cells. Electrical signals were acquired using Axon Instruments Multiclamp 700B amplifier and digitized with Digidata using pClamp acquisition and control software. Gap free recordings were conducted (typically holding the membrane potential at -70 mV) while delivering 100 ms pulses of ultrasound. The ultrasound delivery rig used for patch clamp experiments was the same used for imaging experiments. Briefly, waveforms were programmed using an arbitrary function generator (Keysight Technologies) connected via BC to an amplifier (VTC2057574, Vox Technologies). Military communications grade BNC cables (Federal

Custom Cable) were used to ensure impedance matching in our systems and reduce electrical interference. The amplifier was connected to our custom-made lithium niobate transducer mounted on a dove-tail sliding arm, and coupled to the bottom of the recording chamber with ultrasound gel. The centre of the transducer was left uncoated with gold in order to permit bright-field light to reach the sample, allowing us to align optics and obtain even illumination for DIC imaging. Cell attached experiments with Ex-HEK-GCaMP cells maintained membrane resistances between 0.5 and 3 GΩ. For primary neuron experiments, access resistance during successful whole-cell recordings was required to have ≤15% maximal change.

Viruses. pAAV.Syn.DIO.*hs*TRPA1-myc plasmid was custom made by GenScript. synP.DIO.EGFP.WPRE.hGH was a gift from Ian Wickersham (Addgene viral prep # 100043-AAV9). pAAV.Syn.GCaMP6f.WPRE.SV40[29] was a gift from Douglas Kim & GENIE Project (Addgene viral prep # 100837-AAV9 ; http://n2t.net/addgene:100837 ; RRID:Addgene_100837). pENN.AAV.hSyn.Cre.WPRE.hGH was a gift from James M. Wilson (Addgene viral prep # 105553-AAV9; http://n2t.net/addgene:105553 ; RRID:Addgene_105553). AAV9-hsyn-DIO-*hs*TRPA1-myc (GT3 Core at Salk Institute of Biological Studies) was injected at either 4E13 along with 1E12 AAV9-hsyn-DIO-GFP (Addgene #100043-AAV9) diluted in Hank's Balance Salt Solution for injection. Adult male and female Npr3-cre mice (19-30g) received 400nL unilateral injections to the right motor cortex at AP 0.0 ML -1.0, AP +0.5 ML -1.0, AP +0.5 ML-1.5 at DV 0.5[52]. Briefly, small holes were drilled (0.45 mm drill bit) into the skull over those coordinates, and virus was delivered through a pulled glass pipette at 2nL/sec by a Nanoject iii (Drummond Scientific Company). Successful viral delivery was confirmed post-mortem via immunohistochemistry for GFP and/or the myc-tag.

Mouse primary embryonic neuron culture. For WT primary neuron culture, timed pregnant C57Bl/6 female mice were ordered for E18 cortical dissociation (Charles River: 027). For TRPA1 knockout neuron culture, female TRPA1-/- (JAX #006401) dams were injected with luteinizing hormone releasing hormone (Sigma-Aldrich, L8008) 5 days before being paired with -/- males overnight. Pregnant dams were sacrificed and the E18 embryos were collected for cortical dissociation.

Mouse primary neuronal cultures were prepared from cortices isolated from embryonic day 18 (E18) mice, following the protocol described in[73]. Neurons were plated in 12-well culture plates with 18 mm PDL-coated coverslips (Neuvitro Corporation GG-18-PDL) at a concentration of 600-900k cells/well. Neurons were then incubated at 37°C, 5% CO_2, with half media changes every 2-3 days with Neurobasal (ThermoFisher # 21103049 supplemented with Primocin (InvivoGen #ant-pm-1), B-27 (ThermoFisher # 17504044) and GlutaMAX (ThermoFisher #35050061). For calcium imaging experiments, cells were infected with AAV9-hSyn-GCaMP6f (Addgene #100837-AAV9) at day in vitro 3 (DIV3) and half media change was performed the next day.

Neurons infected with GCaMP6f as stated above were infected with AAV9-hSyn-Cre (Addgene #105553-AAV9) and AAV9-hSyn-TRPA1-myc-DIO (Salk GT3 core) at DIV4 and half media changed was performed the next day. Cultures were incubated at 37°C, 5% CO_2 until DIV10-12 and then imaged using the same equipment as for HEK cell experiments.

Rat primary neuron culture. Rat primary neuronal cultures were prepared from rat pup tissue at embryonic days (E) 18 containing combined cortex, hippocampus and ventricular zone. The

tissue was obtained from BrainBits (Catalogue #: SDEHCV) in Hibernate-E media and used the same day for dissociation following their protocol. Briefly, tissue was incubated in a solution of Papain (BrainBits PAP) at 2 mg/mL for 30 min at 37°C and dissociated in Hibernate-E for one minute using one sterile 9'' silanized Pasteur pipette with a fire polished tip. The cell dispersion solution was centrifuged at 1100 rpm for 1 min, and the pellet was resuspended with 1 mL NbActiv1 (BrainBits NbActiv1 500mL). Cell concentration was determined using a haemocytometer and neurons were plated in 12-well culture plates with 18-mm PDL-coated coverslips (Neuvitro Corporation GG-18-PDL) at a concentration of 1.3 million cells/well. Neurons were then incubated at 37°C, 5% CO_2, performing half media changes every 3-4 days with fresh NbActiv1 supplemented with Primocin™ (InvivoGen ant-pm-1). Neurons infected with GCaMP6f as stated above were infected with AAV9-hSyn-Cre (Addgene #105553-AAV9) and AAV9-hSyn-TRPA1-myc-DIO (Salk GT3 core) at DIV4 and half media changes were performed the next day. Cultures were incubated at 37°C, 5% CO2 until DIV10-12 and were used in electrophysiology experiments.

Calcium imaging analysis. All image analysis was performed using custom scripts written as ImageJ Macros. Cells in the dTom channel were segmented and cell fluorescence over time in the GCaMP channel was measured and stored in csv files. Calcium data was analyzed using custom Python scripts. Calcium signal was normalized as $\Delta F/F$ using a 6s baseline for each ROI and a peak detection algorithm with a fixed threshold of 0.25 was used to identify responsive cells after ultrasound stimulation. For the screen, the number of cells showing a response to ultrasound was calculated as the total percent of responsive cells after 3 consecutive 90 second recordings on the same coverslip. Percent of transfected cells was calculated as the number of

dTom positive cells/total number of cells per field of view imaged . To compare ultrasound response between clones, we used a generalized mixed model, fitting "response" as a Bernoulli response, "clone" as a fixed factor and "cell" as a random effect. Pairwise comparisons were later performed using odds ratios and Tukey method, correcting for multiple comparisons.

Peak amplitude was calculated for each trace as the maximum GCaMP6f ΔF/F value during 60 s after ultrasound stimulation or pharmacological treatment for HEK cells, and 5 s for mouse primary neurons. For the AITC response curve in neurons, mean GCaMP6f ΔF/F up to 1.5 min after adding AITC to the media was used instead of peak amplitude response. For latency and duration analysis in primary neurons, latency of calcium responses was measured as the time to reach 63% of the peak amplitude after stimulation, while width was calculated as the distance between 63% rise and 63% decay. All code used for data analysis can be accessed at https://github.com/shreklab/Duque-Lee-Kubli-Tufail2020.git

Immunocytochemistry. Cells were fixed with 4% paraformaldehyde (PFA) at room temperature for 15 min and subsequently permeabilised by 0.25% Triton X-100 PBS with 5% horse serum. After incubation in blocking solution for 1h at room temperature, cells were incubated overnight at 4°C with different primary antibodies: for HEK cells a mouse monoclonal αTRPA1 antibody (1:1000; Santa Cruz Biotech #376495) was used, while a polyclonal myc antibody (1:1000; Cell Signalling Tech #2272S) was used to detect the tagged channel in primary neuron cultures. Secondary antibody staining was performed at room temperature for 2 h, along with DAPI for 30min. For myc, TSA amplification was performed to increase the signal[74]. Co-localization to the cell membrane was determined via co-transfection and co-immunolabeling with EGFP-CAAX[75], which was a gift from Lei Lu (Addgene plasmid # 86056; http://n2t.net/addgene:86056 ; RRID:Addgene_86056). For cytoskeleton immunolabeling

experiments, fixed cells were incubated with alpha-tubulin antibody (Sigma, #CBL270-I, 1:1000) or phalloidin-488 (ThermoFisher, #A12379, 1:500).

Rotarod. Mouse locomotor behaviour was evaluated on a Rotor-Rod (SD Instruments). Mice underwent a single day of training at a constant speed of 3 RPM to acclimate to the Rotor-Rod. The next day, mice were placed on a rod that started at 0 RPM and gradually increased to 30 RPM over a 5 minute period. The latency to fall off the rod was collected. Each mouse underwent 4 trials daily with a 20 minute inter-trial interval in which mice were returned to their cages. The latency to fall off was averaged across the three best trials. This procedure was repeated across 5 days. The experimenter was blinded as to the identity of groups.

EMG experiments. EMG experiments were conducted between 2-4 weeks after viral injection. EMG data were collected under ketamine (100mg/kg) and xylazine (10mg/kg) anaesthesia from the right and left biceps brachii and right and left biceps femoris through fine wire electrodes (A-M Systems 790700) connected to a PowerLab and BioAmp (AD Instruments). Data were collected at 40k/sec, bandpass filtered from 300 Hz to 1 kHz. Correct electrode placement was confirmed by positive EMG signal in response to pinch. The skin over the skull was opened, and the 6.91MHz lithium niobate ultrasound transducer was coupled to the skull using ultrasound gel (Parker Aquasonic 100). Ultrasound stimuli (1, 10, 100 ms durations) were administered at no less than 10 second intervals at intensities ranging from 0.35-1.05 MPa, intracortical pressure. Visual movement of the right fore or hindlimb in response to stimulation was noted and EMG responses were analysed for latency and duration. Due to the relatively large stimulus artefact from the ultrasound pulse, responses occurring during the ultrasound stimulus could not be

reliably quantified. Therefore, only responses occurring after cessation of the stimulus were considered in our analyses. The experimenter was blinded as to the group during both collection and analysis of the data.

Ultrasound pressure and temperature measurements. Ultrasound pressure and temperature measurements were collected through ultrasound gel at the same position from the face of the lithium niobate transducer and within the brain tissue through the skull using a Precision Acoustics Fibre-Optic Hydrophone connected to a Tektronix TBS 1052B Oscilloscope and ThinkPad Ultrabook. To enable stereotaxic insertion into the brain, the Fibre-Optic Hydrophone probe was carefully threaded through a glass capillary allowing the tip to remain exposed. Cortical measurements were taken in *ex vivo* cranial tissue in which the jaw and palate were removed to expose the base of the brain. Using the centre of the hypothalamus as coordinates 0,0,0, the hydrophone was inserted at AP +1.2, ML 1.0 and lowered to a depth of -5.6 to approximate the location of the layer V motor cortex. The transducer was coupled to the skull via ultrasound gel and temperature and pressure measurements were collected.

Immunohistochemistry and c-fos quantification. At the conclusion of the study, mice were perfused with 0.9% saline followed by 4% paraformaldehyde (PFA) through a peristaltic pump. Brain tissue was immediately collected and incubated in 4% PFA overnight before being changed to 30% sucrose. Tissue was then sectioned at 35 μM into tissue collection solution (glycerine, ethylene glycol, NaH_2PO_4, Na_2HPO_4) and stored at 4 °C. For brain immunohistochemistry, brain sections from ~every 350 μM were immunolabeled for myc (1:500; Cell Signalling 2272S), c-fos (1:500; Encor RCPA-cfos), NeuN (1:1500; Synaptic

Systems 226004), GFP (1:1000; AVES GFP-1010) and DAPI (1:1000). Tyramide amplification was used to enhance the myc and c-fos signals. Briefly, tissue was incubated for 30 min in H_2O_2, blocked for 1 hr in PBST plus 5% horse serum, and then incubated overnight with primary antibodies. The next day, tissue was incubated for 3 hrs at room temp with biotinylated donkey anti-rabbit (1:500, Jackson Immunoresearch 711-065-152), then washed, incubated with ABC (Vector Labs PK-4000) for 30 min, washed, incubated with tyramide[74], washed and incubated with streptavidin conjugated antibody along with secondaries (ThermoFisher Scientific and Jackson Immunoresearch) appropriate to other antigens of interest for 3 hrs at room temp or overnight at 4 °C. Tissue was then mounted onto glass slides and cover slipped with Prolong Gold Antifade mounting medium (ThermoFisher Scientific). Imaging for quantification of *c-fos* and myc expression were conducted at 10x on a Zeiss Axio Imager.M2 connected to an OrcaFlash 4.0 C11440 camera. High quality images depicting myc and fos colocalization with GFP were taken on a Zeiss Airyscan 880 microscope. Imaging of whole brain sections was conducted at 10x on an Olympus VS-120 Virtual Slide Scanning Microscope.

Quantification of c-fos and GFP positive neurons was conducted in FIJI[76] using manual cell counting. c-fos puncta were excluded if they did not colocalize with DAPI. Myc+ GFP+ neurons were also quantified using manual cell counting in FIJI. Only GFP+ cell bodies that were completely filled with myc immunolabeling were considered to be myc+. The experimenter was blinded as to the experimental condition during quantification.

BaseScope. Adult TRPA1 knockout[60] (JAX #006401) and wild-type C57Bl6/J (JAX #000664) mice were perfused with 0.9% saline. A WT C57/Bl6 E18 mouse embryo was also collected from a cohort of embryos slated for dissociation for use in in vitro experiments. Brains and

lumbar DRG were extracted and immediately frozen in OCT. Fresh frozen sections (10um) were direct mounted and slides were stored at -80°C overnight. A custom BaseScope probe (BA-Mm-Trpa1-3zz-st, ACD-Bio Probe Design #: NPR-0003309) targeting 2602-2738 of mouse TRPA1 (NM_177781.5. GTGATTTTT AAAACATTGC TGAGATCGAC CGGAGTGTTT ATCTTCCTCC TACTGGCTTT TGGCCTCAGC TTTTATGTTC TCCTGAATTT CCAAGATGCC TTCAGCACCC CATTGCTTTC CTTAATCCAG ACATTCAG). This region was chosen because it is deleted in the TRPA1 knockout mouse. Tissues were also probed with positive (Ppib, ACD #701071) and negative control (DapB, ACD#701011) probes, which gave the expected results in all experiments. DRG tissue was used as positive control for the TRPA1 probe, as small-diameter DRG neurons are known to express TRPA1. DRGs and cortices from TRPA1 knockout mice were used as a negative control for the TRPA1 probe.

Blood brain barrier experiments. Mice received retro-orbital injections of 10kDa fluorescein isothiocyanate-dextran (Sigma FD10S) at 150mg/mL in saline. Positive control mice immediately received a cortical stab wound with a 27g needle through a small hole drilled at AP 0, ML -1, DV -0.5. Ultrasound-treated mice had their scalp opened and the ultrasound transducer was coupled over the left cortex with ultrasound gel. The transducer delivered 100ms stimuli at 0.88 MPa every 10 seconds for 1 hr. Sham-treated mice underwent the same procedure but the transducer was not turned on. A cohort of mice that did not receive dextran injection or ultrasound was also collected for as a negative control, and all value were normalized to this cohort. (n=4-5 per group, evenly split between male and female). Mice were perfused 70 minutes after cortical injection or start of the ultrasound treatment. One ultrasound-treated mouse had to be omitted from the data set due to inadequate perfusion. Brain sections were

sectioned at 35 µM and processed as floating sections. After blocking, sections were incubated with 647 donkey anti-mouse and DAPI. Images were collected on an Olympus Virtual Slide Scanner (VS-120), using the same settings across all groups. Fluorescein isothiocyanate-dextran 488 and 647-mouse IgG were quantified as mean intensity in left and right cortex from each sample using FIJI. All values were normalized to fluorescent values obtained from samples that received neither dextran nor ultrasound.

Statistics. Statistical analyses were performed in GraphPad Prism and R. All statistical tests in this study were two-tailed. Single-variable comparisons were made with Mann-Whitney test. Group comparisons were made using either analysis of variance (ANOVA) followed by Tukey–Kramer post-hoc analysis or non-parametric Kruskal-Wallis test followed by Dunn's post-hoc analysis. Statistics used to analyse calcium imaging data are described in Methods. No statistical methods were used to predetermine sample sizes for single experiments.

Acknowledgements

We thank Vivian Ko, Daniel Gibbs, Teresa Grider, Josh Nichols, Edward Callaway, Richard Daneman and Ken Diffenderfer, for their technical help; Edward Callaway, Marcos Sotomayor, Kathleen Quach, Javier How, and members of the Chalasani lab for their critical reading of the manuscript. This work was funded by grants from the National Institutes of Health (R01MH111534, R01NS115591), Brain Research Foundation, Innovation grants from Salk Institute and Kavli Institute of Brain and Mind (S.H.C.). C.L-K. is a Vertex Fellow of the Life Sciences Research Foundation. J.F. is grateful for funding from the W.M. Keck Foundation (SERF) in support of transducer design and fabrication for this work. This work was also

supported by the Waitt Advanced Biophotonics and GT3 Cores with funding from NCI CCSG P30014195 and NINDSR24, respectively.

Author contributions

M.D., C.L-K., designed and performed experiments, analysed data and wrote the paper; Y.T., U.G.M., J.M.L., designed and performed experiments and analysed data; E.E. performed bioinformatic analysis; R.S. designed the membrane localization study and established the histology workflow; C.W. performed BaseScope analysis; A.V., and J.F. designed, fabricated and validated ultrasound transducers; and S.H.C. designed experiments and wrote the paper.

Competing interests

The authors declare no competing interests

Additional information

Supplementary Information is available for this paper.

Correspondence and requests for materials should be addressed to S.H.C. (schalasani@salk.edu).

Data availability

The data that support the findings of this study are available from the corresponding author upon reasonable request.

References

1 Deisseroth, K. Optogenetics: 10 years of microbial opsins in neuroscience. *Nat Neurosci* **18**, 1213-1225, doi:10.1038/nn.4091 (2015).

2 Sternson, S. M. & Roth, B. L. Chemogenetic tools to interrogate brain functions. *Annu Rev Neurosci* **37**, 387-407, doi:10.1146/annurev-neuro-071013-014048 (2014).
3 Chen, I. W., Papagiakoumou, E. & Emiliani, V. Towards circuit optogenetics. *Curr Opin Neurobiol* **50**, 179-189, doi:10.1016/j.conb.2018.03.008 (2018).
4 Meister, M. Physical limits to magnetogenetics. *eLife* **5**, doi:10.7554/eLife.17210 (2016).
5 Wheeler, M. A. *et al.* Genetically targeted magnetic control of the nervous system. *Nat Neurosci* **19**, 756-761, doi:10.1038/nn.4265 (2016).
6 Rao, S. *et al.* Remotely controlled chemomagnetic modulation of targeted neural circuits. *Nat Nanotechnol* **14**, 967-973, doi:10.1038/s41565-019-0521-z (2019).
7 Hynynen, K. & Jolesz, F. A. Demonstration of potential noninvasive ultrasound brain therapy through an intact skull. *Ultrasound Med Biol* **24**, 275-283, doi:S0301-5629(97)00269-X [pii] (1998).
8 Clement, G. T. & Hynynen, K. A non-invasive method for focusing ultrasound through the human skull. *Phys Med Biol* **47**, 1219-1236 (2002).
9 King, R. L., Brown, J. R., Newsome, W. T. & Pauly, K. B. Effective parameters for ultrasound-induced in vivo neurostimulation. *Ultrasound Med Biol* **39**, 312-331, doi:10.1016/j.ultrasmedbio.2012.09.009 (2013).
10 Tufail, Y. *et al.* Transcranial pulsed ultrasound stimulates intact brain circuits. *Neuron* **66**, 681-694, doi:10.1016/j.neuron.2010.05.008 (2010).
11 Ye, P. P., Brown, J. R. & Pauly, K. B. Frequency Dependence of Ultrasound Neurostimulation in the Mouse Brain. *Ultrasound Med Biol* **42**, 1512-1530, doi:10.1016/j.ultrasmedbio.2016.02.012 (2016).
12 Folloni, D. *et al.* Manipulation of Subcortical and Deep Cortical Activity in the Primate Brain Using Transcranial Focused Ultrasound Stimulation. *Neuron* **101**, 1109-1116 e1105, doi:10.1016/j.neuron.2019.01.019 (2019).
13 Verhagen, L. *et al.* Offline impact of transcranial focused ultrasound on cortical activation in primates. *eLife* **8**, doi:10.7554/eLife.40541 (2019).
14 O'Brien, W. D., Jr. Ultrasound-biophysics mechanisms. *Prog Biophys Mol Biol* **93**, 212-255, doi:S0079-6107(06)00091-5 [pii]
10.1016/j.pbiomolbio.2006.07.010 (2007).
15 Lee, W. *et al.* Image-guided transcranial focused ultrasound stimulates human primary somatosensory cortex. *Sci Rep* **5**, 8743, doi:10.1038/srep08743 (2015).
16 Lee, W. *et al.* Transcranial focused ultrasound stimulation of human primary visual cortex. *Sci Rep* **6**, 34026, doi:10.1038/srep34026 (2016).
17 Naor, O., Krupa, S. & Shoham, S. Ultrasonic neuromodulation. *J Neural Eng* **13**, 031003, doi:10.1088/1741-2560/13/3/031003 (2016).
18 Tyler, W. J. Noninvasive neuromodulation with ultrasound? A continuum mechanics hypothesis. *Neuroscientist* **17**, 25-36, doi:1073858409348066 [pii]
10.1177/1073858409348066 (2011).
19 Sato, T., Shapiro, M. G. & Tsao, D. Y. Ultrasonic Neuromodulation Causes Widespread Cortical Activation via an Indirect Auditory Mechanism. *Neuron* **98**, 1031-1041 e1035, doi:10.1016/j.neuron.2018.05.009 (2018).
20 Guo, H. *et al.* Ultrasound Produces Extensive Brain Activation via a Cochlear Pathway. *Neuron* **98**, 1020-1030 e1024, doi:10.1016/j.neuron.2018.04.036 (2018).

21 Yoo, S., Mittelstein, D. R., Hurt, R. C., Lacroix, J. J. & Shapiro, M. G. Focused ultrasound excites neurons via mechanosensitive calcium accumulation and ion channel amplification. *bioRxiv* (2020).

22 Kubanek, J., Shukla, P., Das, A., Baccus, S. A. & Goodman, M. B. Ultrasound Elicits Behavioral Responses through Mechanical Effects on Neurons and Ion Channels in a Simple Nervous System. *J Neurosci* **38**, 3081-3091, doi:10.1523/JNEUROSCI.1458-17.2018 (2018).

23 Ibsen, S., Tong, A., Schutt, C., Esener, S. & Chalasani, S. H. Sonogenetics is a non-invasive approach to activating neurons in Caenorhabditis elegans. *Nature communications* **6**, 8264, doi:10.1038/ncomms9264 (2015).

24 Ye, J. *et al.* Ultrasonic Control of Neural Activity through Activation of the Mechanosensitive Channel MscL. *Nano Lett* **18**, 4148-4155, doi:10.1021/acs.nanolett.8b00935 (2018).

25 Qiu, Z. *et al.* The Mechanosensitive Ion Channel Piezo1 Significantly Mediates In Vitro Ultrasonic Stimulation of Neurons. *iScience* **21**, 448-457, doi:10.1016/j.isci.2019.10.037 (2019).

26 Huang, Y. S. *et al.* Sonogenetic Modulation of Cellular Activities Using an Engineered Auditory-Sensing Protein. *Nano Lett* **20**, 1089-1100, doi:10.1021/acs.nanolett.9b04373 (2020).

27 Kubanek, J. *et al.* Ultrasound modulates ion channel currents. *Sci Rep* **6**, 24170, doi:10.1038/srep24170 (2016).

28 Collignon, S., Manor, O. & Friend, J. Improving and Predicting Fluid Atomization via Hysteresis-Free Thickness Vibration of Lithium Niobate. *Advanced Functional Materials* **28**, 1704359 (2018).

29 Chen, T. W. *et al.* Ultrasensitive fluorescent proteins for imaging neuronal activity. *Nature* **499**, 295-300, doi:10.1038/nature12354 (2013).

30 Choy, E. *et al.* Endomembrane trafficking of ras: the CAAX motif targets proteins to the ER and Golgi. *Cell* **98**, 69-80, doi:10.1016/S0092-8674(00)80607-8 (1999).

31 Raisinghani, M. *et al.* Activation characteristics of transient receptor potential ankyrin 1 and its role in nociception. *Am J Physiol Cell Physiol* **301**, C587-600, doi:10.1152/ajpcell.00465.2010 (2011).

32 Eid, S. R. *et al.* HC-030031, a TRPA1 selective antagonist, attenuates inflammatory- and neuropathy-induced mechanical hypersensitivity. *Mol Pain* **4**, 48, doi:10.1186/1744-8069-4-48 (2008).

33 Park, J. *et al.* Screening fluorescent voltage indicators with spontaneously spiking HEK cells. *PLoS One* **8**, e85221, doi:10.1371/journal.pone.0085221 (2013).

34 Wang, Y. Y., Chang, R. B., Waters, H. N., McKemy, D. D. & Liman, E. R. The nociceptor ion channel TRPA1 is potentiated and inactivated by permeating calcium ions. *J Biol Chem* **283**, 32691-32703, doi:10.1074/jbc.M803568200 (2008).

35 Talavera, K. *et al.* Mammalian Transient Receptor Potential TRPA1 Channels: From Structure to Disease. *Physiol Rev* **100**, 725-803, doi:10.1152/physrev.00005.2019 (2020).

36 King, J. V. L. *et al.* A cell-penetrating scorpion toxin enables mode-specific modulation of TRPA1 and pain. *Cell* **178**, 1362-1374. e1316 (2019).

37 Zhao, J., King, J. V. L., Cheng, Y. & Julius, D. Mechanisms governing irritant-evoked activation and calcium modulation of TRPA1. *bioRxiv* (2019).

38 Corey, D. P. *et al.* TRPA1 is a candidate for the mechanosensitive transduction channel of vertebrate hair cells. *Nature* **432**, 723-730, doi:10.1038/nature03066 (2004).

39 Sotomayor, M., Corey, D. P. & Schulten, K. In search of the hair-cell gating spring elastic properties of ankyrin and cadherin repeats. *Structure* **13**, 669-682, doi:10.1016/j.str.2005.03.001 (2005).

40 Zhang, W. *et al.* Ankyrin Repeats Convey Force to Gate the NOMPC Mechanotransduction Channel. *Cell* **162**, 1391-1403, doi:10.1016/j.cell.2015.08.024 (2015).

41 Startek, J. B. *et al.* Mouse TRPA1 function and membrane localization are modulated by direct interactions with cholesterol. *eLife* **8**, doi:10.7554/eLife.46084 (2019).

42 Zidovetzki, R. & Levitan, I. Use of cyclodextrins to manipulate plasma membrane cholesterol content: evidence, misconceptions and control strategies. *Biochim Biophys Acta* **1768**, 1311-1324, doi:10.1016/j.bbamem.2007.03.026 (2007).

43 Cox, C. D. *et al.* Removal of the mechanoprotective influence of the cytoskeleton reveals PIEZO1 is gated by bilayer tension. *Nature communications* **7**, 10366, doi:10.1038/ncomms10366 (2016).

44 Perozo, E., Kloda, A., Cortes, D. M. & Martinac, B. Physical principles underlying the transduction of bilayer deformation forces during mechanosensitive channel gating. *Nat Struct Biol* **9**, 696-703, doi:10.1038/nsb827 (2002).

45 Bae, C., Sachs, F. & Gottlieb, P. A. The mechanosensitive ion channel Piezo1 is inhibited by the peptide GsMTx4. *Biochemistry* **50**, 6295-6300, doi:10.1021/bi200770q (2011).

46 Gnanasambandam, R. *et al.* GsMTx4: Mechanism of Inhibiting Mechanosensitive Ion Channels. *Biophys J* **112**, 31-45, doi:10.1016/j.bpj.2016.11.013 (2017).

47 Hill, K. & Schaefer, M. TRPA1 is differentially modulated by the amphipathic molecules trinitrophenol and chlorpromazine. *J Biol Chem* **282**, 7145-7153, doi:10.1074/jbc.M609600200 (2007).

48 Motter, A. L. & Ahern, G. P. TRPA1 is a polyunsaturated fatty acid sensor in mammals. *PLoS One* **7**, e38439, doi:10.1371/journal.pone.0038439 (2012).

49 Hjerling-Leffler, J., Alqatari, M., Ernfors, P. & Koltzenburg, M. Emergence of functional sensory subtypes as defined by transient receptor potential channel expression. *J Neurosci* **27**, 2435-2443, doi:10.1523/JNEUROSCI.5614-06.2007 (2007).

50 Gouin, O. *et al.* TRPV1 and TRPA1 in cutaneous neurogenic and chronic inflammation: pro-inflammatory response induced by their activation and their sensitization. *Protein Cell* **8**, 644-661, doi:10.1007/s13238-017-0395-5 (2017).

51 Daigle, T. L. *et al.* A Suite of Transgenic Driver and Reporter Mouse Lines with Enhanced Brain-Cell-Type Targeting and Functionality. *Cell* **174**, 465-480 e422, doi:10.1016/j.cell.2018.06.035 (2018).

52 Ueno, M. *et al.* Corticospinal Circuits from the Sensory and Motor Cortices Differentially Regulate Skilled Movements through Distinct Spinal Interneurons. *Cell reports* **23**, 1286-1300 e1287, doi:10.1016/j.celrep.2018.03.137 (2018).

53 Tennant, K. A. *et al.* The organization of the forelimb representation of the C57BL/6 mouse motor cortex as defined by intracortical microstimulation and cytoarchitecture. *Cereb Cortex* **21**, 865-876, doi:10.1093/cercor/bhq159 (2011).

54 FOWLKES, J. B. & HOLLAND, C. K. Section 7: Discussion of the mechanical index and other exposure parameters. *Journal of ultrasound in medicine* **19**, 143-148 (2000).

55 Hayakawa, K., Tatsumi, H. & Sokabe, M. Actin stress fibers transmit and focus force to activate mechanosensitive channels. *Journal of cell science* **121**, 496-503 (2008).

56 Le Roux, A.-L., Quiroga, X., Walani, N., Arroyo, M. & Roca-Cusachs, P. The plasma membrane as a mechanochemical transducer. *Philosophical Transactions of the Royal Society B* **374**, 20180221 (2019).

57 Meseguer, V. *et al.* TRPA1 channels mediate acute neurogenic inflammation and pain produced by bacterial endotoxins. *Nature communications* **5**, 3125, doi:10.1038/ncomms4125 (2014).

58 Jerusalem, A. *et al.* Electrophysiological-mechanical coupling in the neuronal membrane and its role in ultrasound neuromodulation and general anaesthesia. *Acta biomaterialia* (2019).

59 Oh, S. J. *et al.* Ultrasonic Neuromodulation via Astrocytic TRPA1. *Curr Biol* **29**, 3386-3401 e3388, doi:10.1016/j.cub.2019.08.021 (2019).

60 Kwan, K. Y. *et al.* TRPA1 contributes to cold, mechanical, and chemical nociception but is not essential for hair-cell transduction. *Neuron* **50**, 277-289, doi:10.1016/j.neuron.2006.03.042 (2006).

61 Patel, M., Giddings, A. M., Sechelski, J. & Olsen, J. C. High efficiency gene transfer to airways of mice using influenza hemagglutinin pseudotyped lentiviral vectors. *J Gene Med* **15**, 51-62, doi:10.1002/jgm.2695 (2013).

62 Arnadottir, J. & Chalfie, M. Eukaryotic mechanosensitive channels. *Annu Rev Biophys* **39**, 111-137, doi:10.1146/annurev.biophys.37.032807.125836 (2010).

63 Tyler, W. J. The mechanobiology of brain function. *Nat Rev Neurosci* **13**, 867-878, doi:10.1038/nrn3383 (2012).

64 Syeda, R. *et al.* Chemical activation of the mechanotransduction channel Piezo1. *eLife* **4**, doi:10.7554/eLife.07369 (2015).

65 Chu, Y., Cohen, B. E. & Chuang, H. H. A single TRPV1 amino acid controls species sensitivity to capsaicin. *Sci Rep* **10**, 8038, doi:10.1038/s41598-020-64584-2 (2020).

66 Cui, M. *et al.* TRPV1 receptors in the CNS play a key role in broad-spectrum analgesia of TRPV1 antagonists. *J Neurosci* **26**, 9385-9393, doi:10.1523/JNEUROSCI.1246-06.2006 (2006).

67 Hofer, A. M. Another dimension to calcium signaling: a look at extracellular calcium. *J Cell Sci* **118**, 855-862, doi:10.1242/jcs.01705 (2005).

68 Lee, C. H. & Ruben, P. C. Interaction between voltage-gated sodium channels and the neurotoxin, tetrodotoxin. *Channels (Austin)* **2**, 407-412, doi:10.4161/chan.2.6.7429 (2008).

69 Katoh, K. & Standley, D. M. MAFFT multiple sequence alignment software version 7: improvements in performance and usability. *Molecular biology and evolution* **30**, 772-780 (2013).

70 Stamatakis, A. RAxML version 8: a tool for phylogenetic analysis and post-analysis of large phylogenies. *Bioinformatics* **30**, 1312-1313 (2014).

71 Fantini, J. & Barrantes, F. J. How cholesterol interacts with membrane proteins: an exploration of cholesterol-binding sites including CRAC, CARC, and tilted domains. *Front Physiol* **4**, 31, doi:10.3389/fphys.2013.00031 (2013).

72 Rice, P., Longden, I. & Bleasby, A. EMBOSS: the European Molecular Biology Open Software Suite. *Trends Genet* **16**, 276-277, doi:10.1016/s0168-9525(00)02024-2 (2000).

73 Hilgenberg, L. G. & Smith, M. A. Preparation of dissociated mouse cortical neuron cultures. *J Vis Exp*, 562, doi:10.3791/562 (2007).

74 McKay, J. A., Murray, G. I., Keith, W. N. & McLeod, H. L. Amplification of fluorescent in situ hybridisation signals in formalin fixed paraffin wax embedded sections of colon tumour using biotinylated tyramide. *Mol Pathol* **50**, 322-325, doi:10.1136/mp.50.6.322 (1997).

75 Madugula, V. & Lu, L. A ternary complex comprising transportin1, Rab8 and the ciliary targeting signal directs proteins to ciliary membranes. *J Cell Sci* **129**, 3922-3934, doi:10.1242/jcs.194019 (2016).

76 Schindelin, J. *et al.* Fiji: an open-source platform for biological-image analysis. *Nat Methods* **9**, 676-682, doi:10.1038/nmeth.2019 (2012).

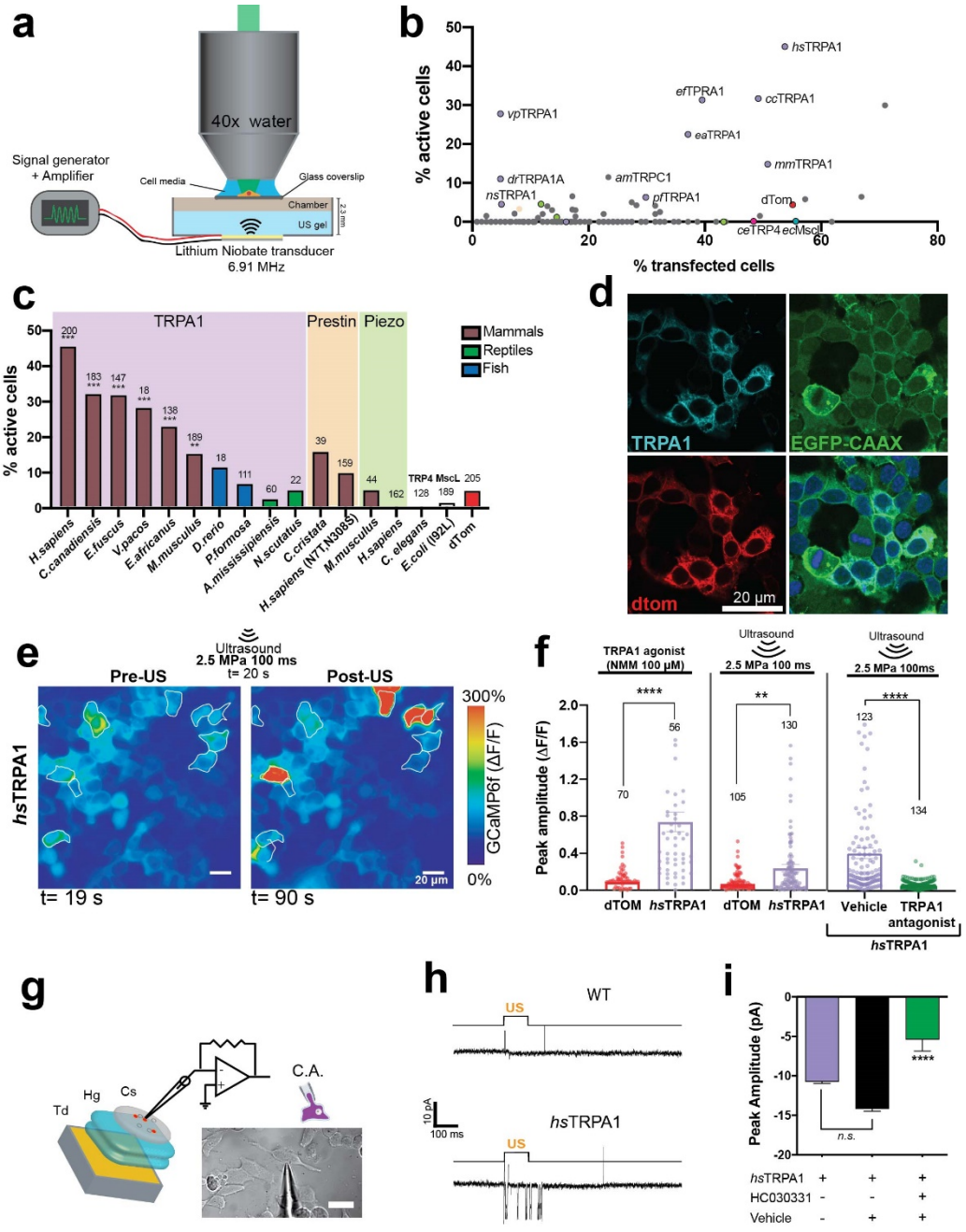

Figure 1 | *hs*TRPA1 confers sensitivity to single, short duration ultrasound pulses in HEK cells a, Schematic showing the 6.91 MHz lithium niobate transducer delivering ultrasound stimuli to cells. Plot showing **b,** the percent of transfected vs active cells after ultrasound stimulation for 191 cDNAs and **c,** the top responders and their homologs compared to previously published ultrasound-sensitive candidates. **d,** Representative image showing *hs*TRPA1 expression co-localized with membrane-targeted EGFP-CAAX in HEK cells. **e,** Change in GCaMP6f fluorescence in HEK cells expressing *hs*TRPA1 upon ultrasound

stimulation. ROIs identify transfected cells (dTom+). Scale bar 20μm. GCaMP6f peak amplitude in *hs*TRPA1- or dTom–expressing (control) HEK cells stimulated with **f,** TRPA1 agonist (NMM, 100 μM), ultrasound alone or TRPA1 antagonist (HC-030031 40 μM.). **g,** Schematic showing the cell-attached configuration for electrophysiology with a DIC image of a representative HEK cell. **h,** Representative gap-free voltage-clamp trace of dTom control- or *hs*TRPA1-expressing HEK to 100 ms, 2.5 MPa ultrasound stimuli. i**,** Mean peak amplitude (pA) from HEK cells expressing *hs*TRPA1 alone, and *hs*TRPA1 treated with vehicle or TRPA1 antagonist (HC-030301 40 μM). Numbers of cells analysed is indicated above each bar. **c,** **p < 0.01, ***p<0.001, ****p<0.0001 by logistic regression, **f, i,** **p < 0.01, ****p<0.0001 by Mann-Whitney test.

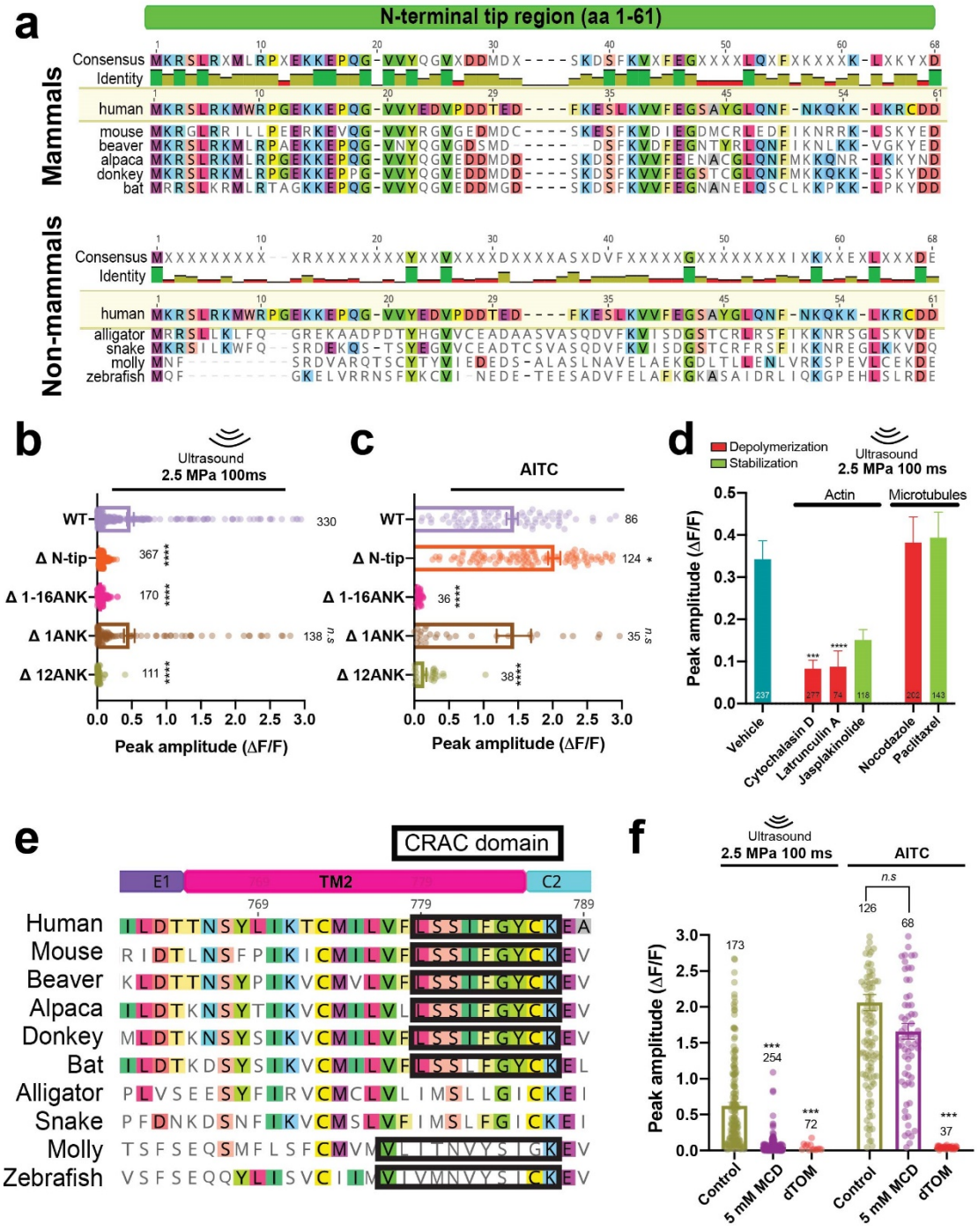

Figure 2 | *hs*TRPA1 domains that contribute to activation by ultrasound. a, Mammalian and non-mammalian alignments of the TRPA1 N-terminal tip region (aa1-61) from homologs tested for ultrasound sensitivity. GCaMP6f peak amplitude upon **b,** ultrasound stimulation or **c,** treatment with AITC **(**33 μM) in HEK cells transfected with either full-length hsTRPA1 or channels containing deletions of the N-terminal tip (ΔN-tip), ankyrins 1-16 (ΔANK1-16), ankyrin 1(ΔANK1) or ankyrin 12 (ΔANK12) without altering the pore or transmembrane regions. **d,** GCaMP6f peak amplitude following ultrasound stimulation in cells expressing hsTRPA1 after treatment with agents that either stabilize (green) or destabilize (red) microtubules and actin filaments compared to vehicle control. **e,** Transmembrane 2 domain sequence alignment across species tested for ultrasound sensitivity with Cholesterol Recognition/interaction Amino acid Consensus (CRAC) domains outlined. **f,** GCaMP6f peak amplitude in *hs*TRPA1-expressing HEK cells upon ultrasound stimulation or AITC treatment (33 μM) after incubation with MCD (5 mM) or control; Numbers on each bar indicate numbers of cell analysed. $p>0.05$, $^{**}p<0.01$, $^{***}p<0.001$, $^{****}p < 0.0001$ by Kruskal-Wallis rank test and Dunn's test for multiple comparisons.

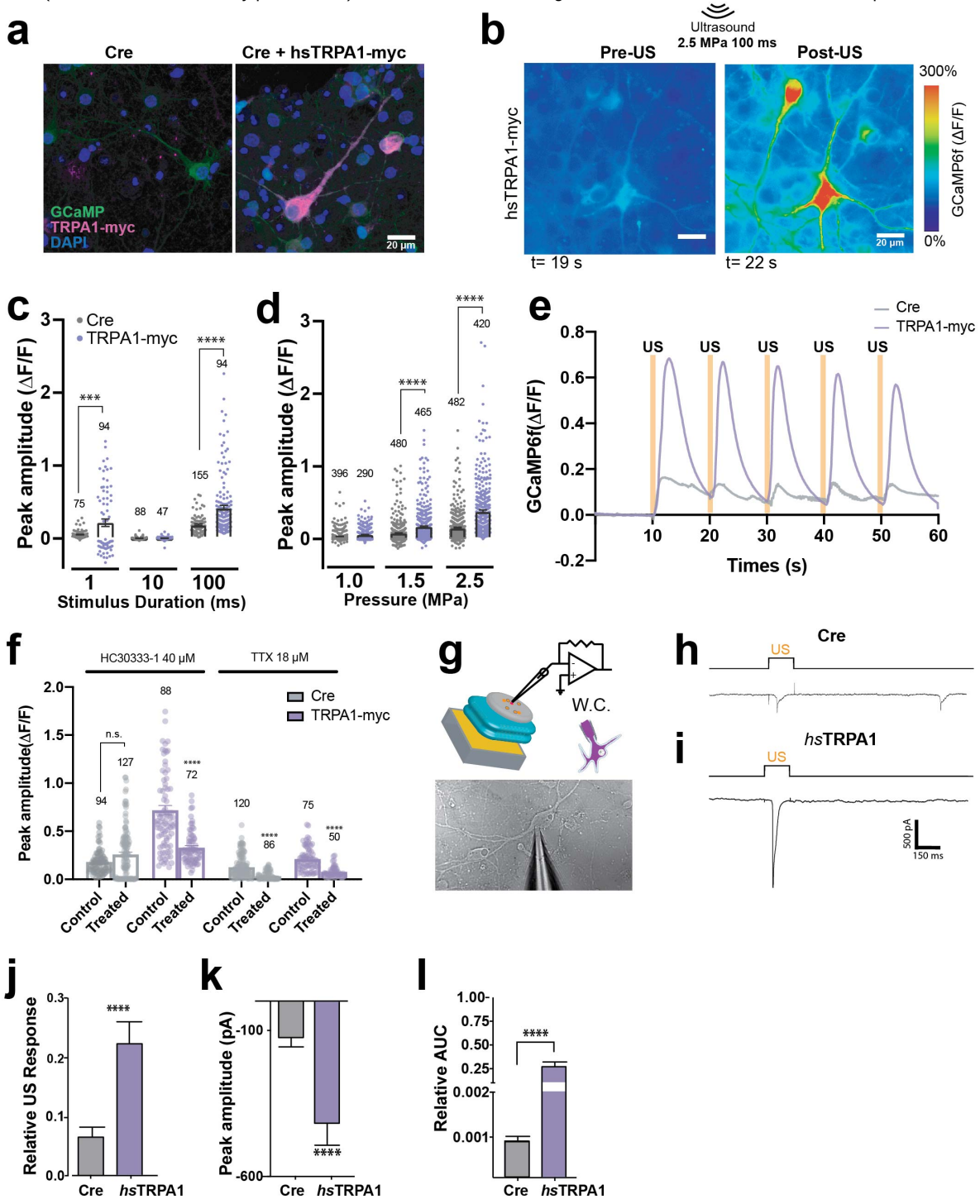

Figure 3 | *hs*TRPA1 potentiates ultrasound responses in rodent primary neurons *in vitro*. Representative images showing mouse primary neurons **a,** expressing *hs*TRPA1 or controls; **b.,** and change in GCaMP6f fluorescence in *hs*TRPA1 expressing neurons upon ultrasound stimulus. Plots showing peak amplitude of GCaMP6f fluorescence upon **d,** 2.5 MPa ultrasound stimuli of different stimulus durations and e, 100 ms ultrasound stimuli at various peak negative pressures. **e,** Average ratio of change in fluorescence to baseline fluorescence in neurons expressing *hs*TRPA1 or control plasmids during repetitive 100 ms, 2.5 MPa ultrasound stimulation. **f,** Plot showing GCaMP6f peak amplitude in *hs*TRPA1 neurons or controls treated with TRPA1 antagonist (HC-030031, 40 μM) or TTX (tetrodotoxin, 18 μM). **g,** Schematic showing whole cell patch electrophysiology of neurons expressing *hs*TRPA1. Representative gap-free voltage-clamp traces of **(h)** control or **(i)** neurons expressing *hs*TRPA1 upon ultrasound stimuli. Plots showing **(j)** relative ultrasound responses, **(k)** peak amplitude, and **(l)** area under the curve in neurons expressing *hs*TRPA1 or controls (Cre). The number of GCaMP6f-expressing neurons analysed is indicated above each bar. **c,** **** $p<0.0001$, by Mann-Whitney U test; **d-g,** * $p<0.05$, ** $p<0.01$, ****$p<0.0001$ by two-way ANOVA with Geisser-Greenhouse correction. **k-m,** ****$p<0.0001$ by unpaired, two-tailed Mann-Whitney U test.

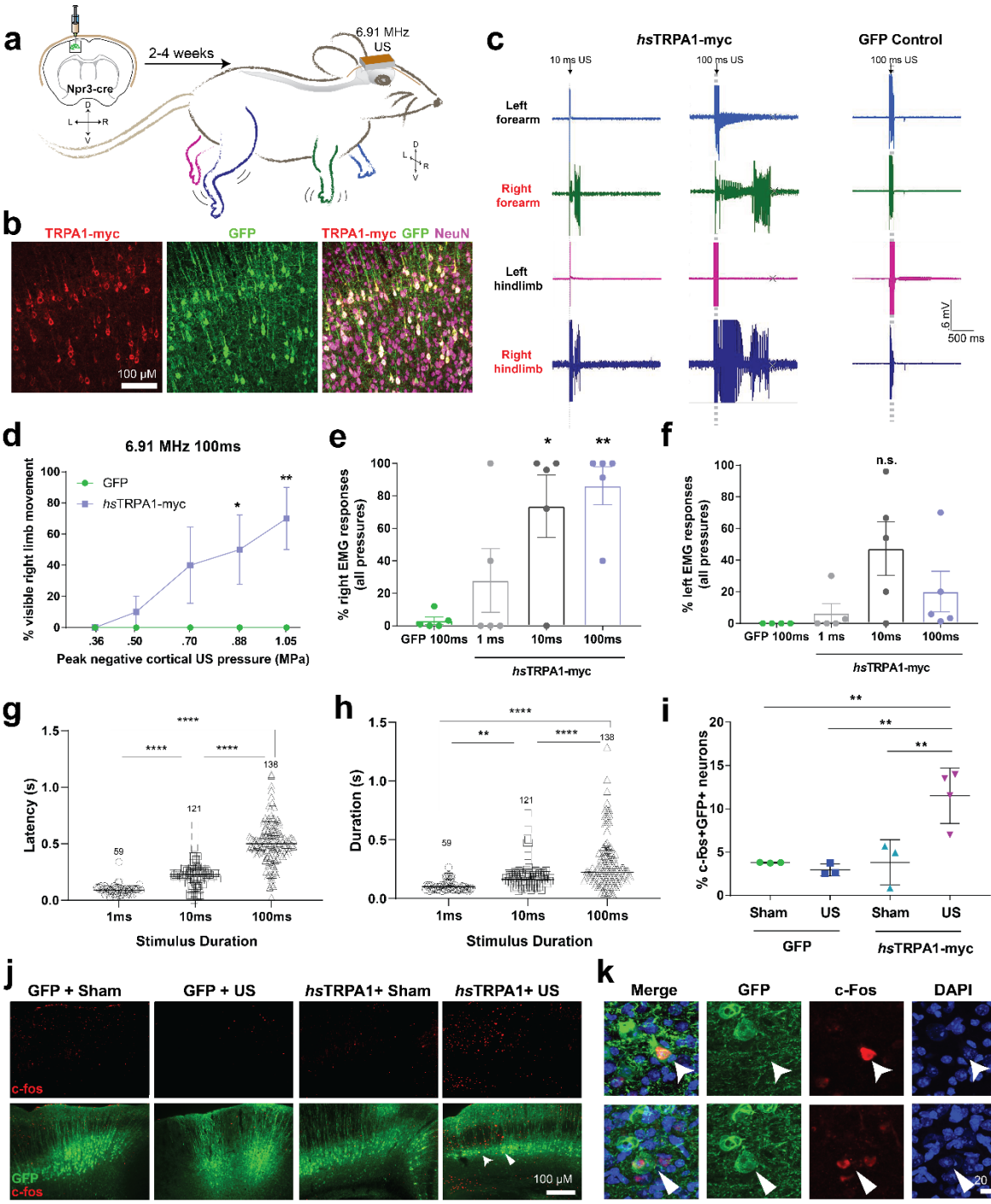

Figure 4 | hsTRPA1 enables sonogenetic activation of mouse layer V motor cortex neurons *in vivo.* **a,** Schematic showing expression of *hs*TRPA1 or GFP controls in the left motor cortex of Npr3-Cre transgenic mice innervating the right fore and hindlimbs allowing these to be controlled with ultrasound stimuli. **b,** Images showing expression of *hs*TRPA1 and GFP (co-injection marker) in layer 5 cortical neurons *in vivo*. **c,** Representative EMG responses to 10 ms and 100 ms ultrasound stimuli from animals expressing *hs*TRPA1 and controls. **d,** Visible right limb movements were scored in response to 100 ms ultrasound pulses of varying intensities. Plots showing percent of **(e)** right fore and hindlimb and (**f)** left fore and hindlimb EMG responses relative to number of stimulations pooled across all intensities. Plots showing **(g)** latency between the start of the ultrasound pulse and subsequent EMG response, and (**h)** duration from the start of the EMG response until the signal returned to baseline. **i,** Percent of c-fos+ GFP+ neurons quantified from sections taken at ~700 μM intervals throughout the GFP+ region of the cortex. Representative images showing co-localization of **j,** c-fos and GFP and **k,** c-fos and DAPI within GFP positive neurons. **d - f,** n = 5/group, **g- h,** n = 39-138, **i,** n = 3-4/group *p<0.05, **p<0.01, ****p<0.0001 compared to GFP control by two-way ANOVA followed Tukey's multiple comparisons.